Journal of Petroleum Science and Engineering 214 (2022) 110470

Contents lists available at ScienceDirect

Journal of Petroleum Science and Engineering

journal homepage: www.elsevier.com/locate/petrol

Modeling of subsurface sedimentary facies using Self-Attention Generative Adversarial Networks (SAGANs)

Mei Chen [a,b], Shenghe Wu [a,b,*], Heather Bedle [c], Pengfei Xie [a,b], Jiajia Zhang [a,b], Yunlong Wang [a,b]

[a] State Key Laboratory of Petroleum Resources and Prospecting, China University of Petroleum (Beijing), Beijing, 102249, China
[b] College of Geosciences, China University of Petroleum (Beijing), Beijing, 102249, China
[c] School of Geosciences, University of Oklahoma, Norman, OK, USA

ARTICLE INFO

Keywords:
Sedimentary facies modeling
Machine learning
Convolution processes
SAGANs
Distribution pattern

ABSTRACT

Understanding subsurface distribution features is crucial for reliable sedimentary facies modeling. Obtaining the distribution feature of complex subsurface sedimentary facies is challenging, especially non-stationary sedimentary facies which are location-specific, well-ordered, facies sequence (e.g., deltas). The application of machine learning algorithms has potential to assist with this imaging problem, particularly using the Generative Adversarial Networks (GANs) method. Recently, GANs have proven to be outstanding for unsupervised learning on complex distributions of training images. However, in most GAN-based model convolution processes, the information in a local area is computationally invalid for reproducing the global features of training images. To remedy this, we introduce an advanced Self-Attention Generative Adversarial Network (SAGAN) for subsurface geological facies modeling. Compared with the basic GANs, SAGANs introduce a self-attention mechanism to attain details from a long distance in the image, reproducing global features of training images. SAGAN case studies involve stationary channels and non-stationary delta facies. We use probability maps, variograms, connectivity functions, and visualization results to evaluate and compare our simulation realizations. For channel cases, SAGANs' realizations can reproduce different distributions of channels and point bars in different river systems. For the delta case, the SAGAN method shows a better ability to reproduce delta non-stationary characteristics than the MPS and basic GAN methods. All results are of high quality and diversity, reproduced the known geological sedimentary patterns, and compared with the basic GANs, SAGANs can better reproduce the global features of non-stationary training images. It is demonstrated that our first proposed SAGANs for geological facies modeling represent a powerful method for reproducing depositional facies distribution pattern.

1. Introduction

Sedimentary facies modeling has become an important part of reservoir development, laying an important foundation for reservoir numerical simulation. A high-quality model that can characterize the subsurface sedimentary facies distribution improves development plans and reduces costs. However, there are some problems in the existing sedimentary facies modeling method, and it is difficult to acquire a reliable model. In particular, the subsurface distribution characterization in models does not reproduce prior known sedimentary facies distribution pattern, including shape, direction and connectivity of sedimentary facies and so on. (Laloy et al., 2017; Li et al., 2016; Tian et al., 2019).

Subsurface sedimentary facies modeling research usually relies on stochastic simulation methods to reproduce the underground structure. One commonly adopted choice is multiple-point statistics (MPS) simulation, which characterizes the spatial correlation of multiple points in space (Strebelle, 2002; Caers and Zhang, 2002; Wu et al., 2007; Feng et al., 2017a; Mariethoz et al., 2010). MPS infers the correlation between multiple spatial points from the training image (TI) to predict the real reservoir (e.g., geologic facies). Despite new progress (Laloy et al., 2016; Wang et al., 2018), MPS simulation without any processing (partition simulation, scaling and rotating training image, etc.) is slow and it is difficult to reproduce the real spatial structure of TI (for example, insufficient continuity), especially for complex facies with non-stationary characteristics. Thus, building effective reservoir models

* Corresponding author. College of Geosciences, China University of Petroleum-Beijing, Beijing, 102249, China.
E-mail address: reser@cup.edu.cn (S. Wu).

https://doi.org/10.1016/j.petrol.2022.110470
Received 24 July 2021; Received in revised form 5 February 2022; Accepted 25 March 2022
Available online 4 April 2022

that satisfies the distribution characteristics of sedimentary facies is an unsolved, important research problem.

The fast-growing field of machine learning (ML) is increasingly promising for accelerating progress (Bergen et al., 2019). The generative model is a type of ML methodology that can be described as a model for generating data, such as a type of probability model. Recent studies have widely explored the application of deep generative models, particularly GANs (Goodfellow et al., 2014). In the last few years, a GAN has been recognized as one of the most advanced ML methods in generative models for capturing complex distributions (Goodfellow et al., 2014). GANs have recently been applied in earth sciences, especially finding success in reservoir modeling (for example, Zhang et al., 2019; Song et al., 2021a, 2021b, 2021c, 2021d).

Many geologists and computer scientists have successfully applied the GAN method for sedimentary facies modeling. Chan and Elsheikh (2017) applied GANs to generate subsurface facies models with realistic, complex geological structures. Laloy, Hérault (2017) proposed spatial GANs (SGANs) and used SGANs for probabilistic inversion involving 2-D and 3-D sedimentary facies. Mosser, Dubrule (2017, Mosser et al., 2018) the generated spatial structure of porous media and micro-CT oolitic limestone with DCGANs. Dupont et al. (2018) used a GAN with image inpainting, to predict the sedimentary facies distribution in river environments from the existing rock type data. Veillard et al. (2018) interpreted geological structures in 3-D seismic data with a GAN and a VAE (Kingma and Welling, 2013). Zhang et al. (2019) also generated geologically realistic 3-D reservoir facie models with GANs. Liu et al. (2020) used perceptual GANs to enhance the resolution of a large field of view image for sandstone thin-section images. Canchumuni et al. (2019) used GANs to develop conditional modeling for facies matching.

However, there are still some problems in GANs facies modeling applications. The objectives of existing tests are mostly simple and homogeneous training images (e.g. channels), and some complex and heterogeneous images are rarely taken into consideration (e.g. deltas). These images can be divided into two types, stationary and non-stationary images. Stationary is invariant by any translation. Non-stationary is the opposite of stationary. Generally, the channel depositional system is stationary facies, because its sedimentary characteristics are similar in all parts of the entire depositional area. Delta depositional system is considered to be non-stationary facies, because their distribution has variable directionality and obvious tendency, i.e. the channel of delta gradually expands outward, showing a fan-like radial shape, which means their distribution is too location-specific and its patterns are not repeated over the whole depositional area. Moreover, most researchers only combine convolution and GANs to learn the features of training images, and it is difficult to learn the global features only by convolution process of most GANs. Despite recent advances in using the GAN method for geology (Zhu and Zhang, 2019; Zhang et al., 2021; Song et al., 2021a, 2021b, 2021c,2021d), all GAN-based models in reservoir modeling (Radford et al., 2015; Karras et al., 2017) are constructed using convolutional layers. Convolutions process and characterize the features of information in local neighborhoods, resulting in the GAN's output solely relating to small areas in the image, and invalid with any other parts. Thus, it is computationally inefficient to use convolutional layers alone to reproduce the global features of the TIs.

To remedy this limitation, a Self-Attention Generative Adversarial Network (SAGAN, Zhang et al., 2019) is introduced in our application. SAGANs add a self-attention module into convolutional GANs, capturing details from a long distance in the image, thereby improving the perception field to obtain global information of the training image. Deep convolutional self-attention GANs are used herein for the generation of sedimentary facies facies systems. We test the SAGANs performance in a case study of stationary channel facies and non-stationary delta sedimentary facies from the Stanford public reservoir data, representing sedimentary facies features in generally recognized representative sedimentary environments of rivers and deltas (Lee and Mukerji, 2012; Feng et al., 2017b). For channel facies, we simulate four facies: point bars, channels, floodplains facies. For delta facies, we simulate two facies: channels and floodplains.

This paper is organized as follows. Section 1 mainly introduces and summarizes the research progress of sedimentary facies modeling and GANs. Section 2 introduces a self-attention GAN architecture compared to most based GANs, and generates quality assessment methods for SAGANs realizations. Section 3 represents the subsurface sedimentary facies simulation results, including channel facies and delta facies cases to demonstrate our proposed SAGAN's capability with quality assessments. In Section 4, we discuss the advantages and limitations of our method's application and outline possible sedimentary facies future for developments in the future. Finally, Section 5 concludes the paper with a summary of the most important findings.

2. Methodology

2.1. Self-attention GANs architecture

A GAN is a deep learning model and one of the most promising methods for unsupervised learning on complex distributions in recent years. The model produces realistic output through mutual game learning of two modules in the framework: generative model and discriminative model. Our proposed SAGAN method is an important development of GANs. Compared to most GAN-based image generation, SAGANs apply the attention mechanism to the GANs generation task, mainly multiplying each feature map with its own transposition, to ensure that the pixels at any two positions are directly related. Therefore, it can learn the difference between any two pixels dependency relationships to obtain global characteristics. SAGANs make up for the shortcomings of the inefficiency of convolutional layers obtaining relations from distant regions, due to the convolution process having a local receptive field. Our sedimentary facies modeling is an extended application of SAGANs by Zhang et al. (2021). We used this method to test different types of sedimentary facies and apply this method to our sedimentary facies modeling.

Self-attention effectively improves the long-range dependency modeling. The image feature is calculated as the attention map in SAGANs (Fig. 1) after the previous layer x is convolved to feature spaces p(x), q(x). Moreover, a parameter $\theta_{j,i}$ indicating the extent of the attention that is added, which refers to the model weight of the i^{th} location when generating the j^{th} area as follows:

$$\theta_{j,i} = \frac{\exp\left(t_{ij}\right)}{\sum_{i=1}^{N} \exp\left(t_{ij}\right)}, \text{ where } t_{ij} = \mathrm{p}(x_i)^T \mathrm{q}(x_j),\ \mathrm{p}(x_i) = W_p x_i,\ \mathrm{q}(x_i) = W_q x_i \quad (1)$$

where, $W_p = R^{\overline{M}\times M}$, and $W_q = R^{\overline{M}\times M}$ are learned weight parameters and M is the number of channel and feature locations. ($\overline{M} = M/8$, according to Zhang et al. (2021)).

The output of the attention module is $\mathrm{e} = (e_1, e_2, \ldots, e_j, \ldots, e_N) \in R^{M\times N}$, where M and N are the number of channel and feature locations. Here, Equation (2) is as follows:

$$e_j = s\left(\sum_{i=1}^{N} \theta_{j,i} k(x_i)\right),\ \mathrm{k}(x_i) = W_k x_i,\ \mathrm{s}(x_i) = W_s x_i. \quad (2)$$

where $k(\mathrm{x})$ is the feature space of which x is convolved, and $W_k = R^{\overline{M}\times M}$, $W_s = R^{\overline{M}\times M}(\overline{M} = M/8)$, are learned weight parameters, implemented as 1×1 convolutions. $\otimes$ denotes matrix multiplication and the softmax operation is performed on each row. Finally, the output above is first multiplied by the scale parameter, and then added to the input feature map x. In SAGANs, both the generator and the discriminator use the attention module.

It is trained in an alternating adversarial way through the following loss function in both the generator and discriminator as follows:

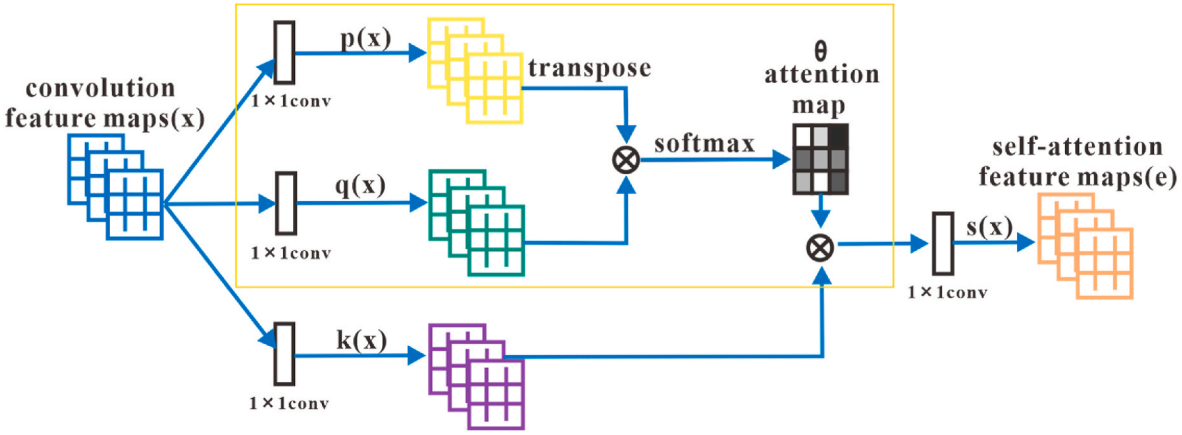

Fig. 1. The self-attention module of SAGANs. The yellow box is part of the self-attention mechanism (Modified from Zhang et al., 2019). (For interpretation of the references to colour in this figure legend, the reader is referred to the Web version of this article.)

$$L_D = -E_{(x,y)\sim P_{data}}[\min(0,-1+D(x,y))] - E_{z\sim P_z,\ y\sim P_z}[\min(0,-1-D(G(z),y))],$$
$$L_G = -E_{z\sim P_z,\ y\sim P_{data}} D(G(z),y) \tag{3}$$

here, $z \sim P_z$, and $y \sim P_{data}$ are our given random vector z and the input data distribution. For all models, we use the Adam optimizer (Kingma and Ba, 2014) for training.

2.2. Generation quality assessment

The quality assessment of the generated model is necessary when applying the SAGAN method to sedimentary facies modeling. For sedimentary facies modeling, it is necessary to evaluate the similarity between the realization and the spatial characteristics of the training image. Therefore, some assessment metrics are applied to evaluate the generation ability. For each example, the probability maps, variogram function and connectivity function are calculated as structural evaluation indicators.

2.2.1. Probability calculation

To compare the similarity between the realizations and the training images, we calculate their probability maps to reflect whether the image positions with higher probability are similar. In detail, we select the same number and similar images to determine the probability of a certain facies, as well as the ratio of frequency of the facies in each position of the image to the total.

2.2.2. Indicator variogram

The variogram is used to describe the spatial diversification of properties, which can quantitatively describe the spatial correlation of regionalized variables, and is widely used in the study of spatial correlation in geostatistics. Generally, half of the variance of geological variables at two positions (with a distance h) in space is defined as the variogram. The variogram is calculated as follows:

$$\gamma(\mathrm{h}) = \frac{1}{2}E\left[(I(x) - I(x+h))^2\right] \tag{4}$$

and $I(x)$ is the indicator function of the facies. The variogram is used in our cases as an indicator of the spatial correlation of the facies in the reservoir models.

2.2.3. Connectivity function

To compute the function for a given value for a discrete image, it is possible to shift one copy of the image and check the number of overlapping pixels of the same category (label) and the number of pixels of the same component. Dividing number of the pixels of the same component by the number of pixels of the same category gives the connectivity function for the given h (two positions with distance h). The connectivity functions $\tau_i(h)$ are is defined as the probability that two pixels belong to the same connected component, and i is the facies indicator as follows:

$$\tau_i(h) = P[x \leftrightarrow x+h | I(x) = i] \tag{5}$$

We use the connectivity function to evaluate the continuity of the reservoir facies, and compare the calculated curves of the variogram and connectivity functions on each realization belonging to the training set and the simulation set. Models are randomly selected for the performed curve comparison evaluation.

3. Subsurface sedimentary facies' simulation results

Our TIs are from the Stanford VI-E reservoir (Lee and Mukerji, 2012) (and available at https://github.com/SCRFpublic/Stanford-VI-E/tree/master/Facies). The Stanford VI-E reservoir models without structural fluctuations are used as TIs (Fig. 2). The reservoir is a fluvial channel system with three layers prograding, layer 3, layer 2, and layer 1 from bottom to top (Castro et al., 2005). In the fluvial system (Fig. 2(a)), deltaic deposits (layer 3, Fig. 2(d)) are deposited first, followed by meandering channels (layer 2, Fig. 2(c)), and later -sinuous channels are formed (layer 1, Fig. 2(b)). These are further discussed below.

3.1. Channel facies (stationary facies)

Our first channel facies test case considers the 150×200 channelized TIs (sinuous channels, layer 1) depicted in Fig. 2(b) as a representative of sedimentary facies with stationary features. The sinuous channels contain four facies: point bars, channels with sand deposits, floodplains and boundaries (flow boundaries) with shale deposits. We use eighty vertical layers of the three-dimensional channel deposition as the TIs.

The size of all generated SAGAN models is designed to be 64×64. At maximum epoch 95 of training, the SAGANs model considered optimal is realized (see parameters in Tables A1-A2 and Figures A1-A3 in Appendix). It takes approximately 3 h to train SAGANs for 95 epochs on an Intel(R) Xeon(R) Gold 5122 CPU. while it takes 0.04 s to generate a single 64×64 implementation using the trained network.

Fig. 3 displays five random selection realizations and five TIs with a size of 150×200, accompanied by the probability maps of green channel of facies 2. Visually, the realizations appear reasonably in agreement with the TIs. The shapes of the channel and the point bar are consistent with geology. The stacking relationship between the channel and the point bar is realistic; along the convex inner edges of the meanders of channels, point bar deposits occur. For the discrete yellow edge facies,

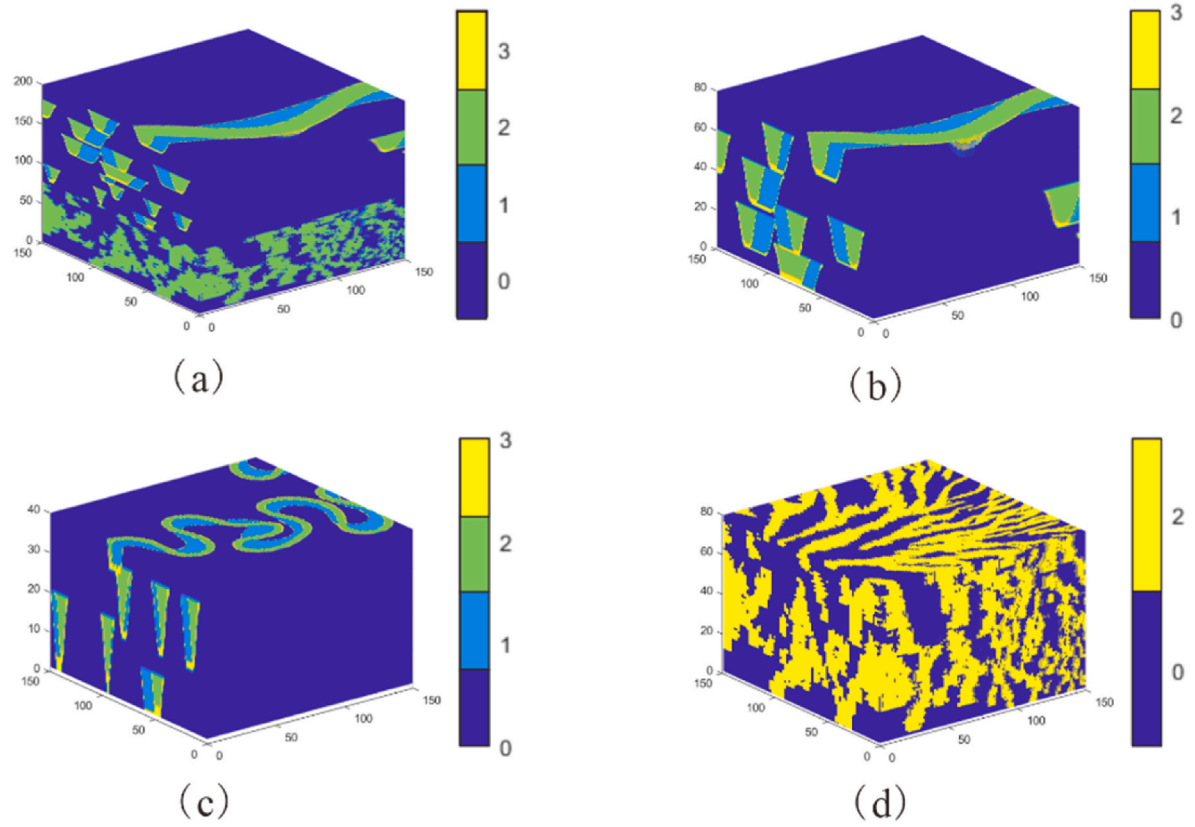

Fig. 2. TIs for SAGANs simulation. Models of Stanford VI without structural fluctuations (a); sinuous channels (layer 1): (b); meandering channels (layer 2): (c); and deltaic deposits (layer 3): (d). 0: floodplain, 1: point bar, 2: channel, 3: boundary (Modified from Castro et al., 2005).

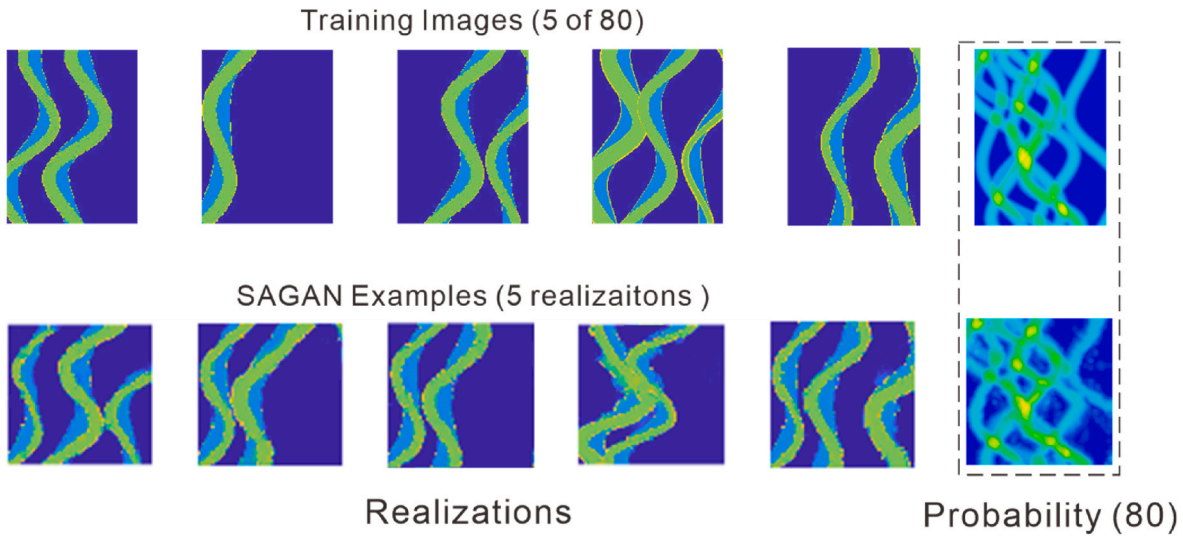

Fig. 3. Five randomly chosen TIs and realizations of sinuous channels, along with corresponding probability maps of green channel facies. (For interpretation of the references to colour in this figure legend, the reader is referred to the Web version of this article.)

the yellow facies realized by SAGANs are also distributed on the edges of other facies; Additionally, the appearance of relatively narrow edge yellow facies at the bottom of the water channel, the realizations can also reproduce the characteristics of the channel. Simultaneously, sand deposits have different expression manifestation, including: differences in the combination of various channels, deposition ratios, channel widths and curvatures, point bar widths, etc. Moreover, a probability map (bottom) of the green channel (facies 2) is calculated from 80 simulation results similar to the training image (top), which is highly consistent with the probability map of the training image. In the probability maps, the high probability locations of the channels are similar, and both show a trend of lower marginal probability.

Fig. 4 shows the corresponding variogram and connectivity functions of channel facies 2 in three directions. Since facies 0, 1 and 3 are not continuous in the entire deposition area, the variograms of these facies are supplemented in the appendix. Our results fluctuate slightly in the variogram of the training image. The mean curve (red) of the realizations is very close to TI mean (black), especially in the X and Y

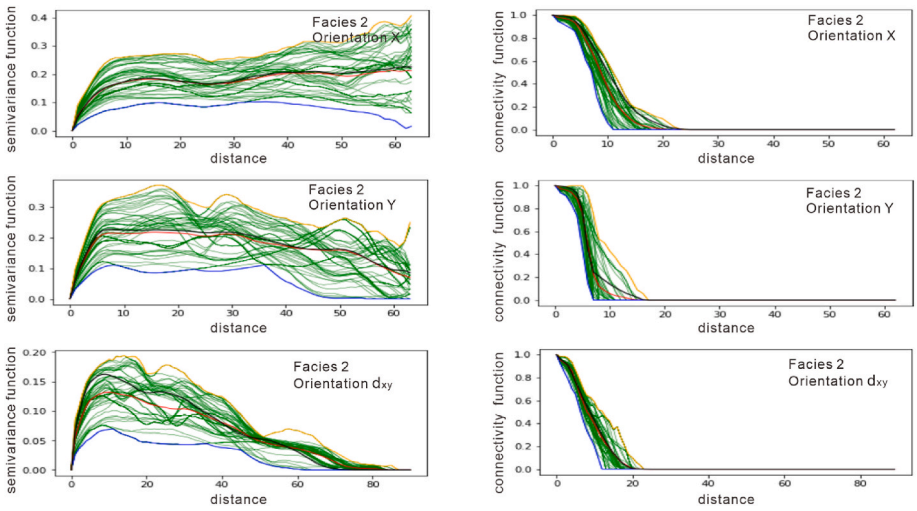

Fig. 4. Variograms and connectivity functions for layer 1 sinuous channels. The black line refers to the mean at each distance to 80 TIs of size64 × 64 from the 200 × 150. The green lines are 80 realizations of size 64 × 64, and the red lines are the mean of these green lines. The yellow and blue lines represent the maximum and minimum values of the function corresponding to the realizations. We calculate the functions for facies 2 along three main directions: x axis, y axis, and d_{XY} (45° direction). (For interpretation of the references to colour in this figure legend, the reader is referred to the Web version of this article.)

directions. The average deviation is not more than 0.2. This shows the similarity between the realizations and TIs at a two-point relation and assists in explaining the realistic simulation realization. For the connectivity function, by comparing the mean curve (red) of the realizations and TIs (black), the realizations match well with the TIs, and the maximum absolute deviation is 0.2. The rapid downward trend of the connectivity function itself also shows that the continuity achieved by our simulation is good, which is consistent with continuous channel deposition.

The second channel test case considers the 150×200 channelized TIs (layer 2) depicted in Fig. 2(c), as another representative sedimentary facies with stationary features. The TIs are meandering channels, deposited in this fluvial channel system. Meandering channels contain four facies as sinuous channels: floodplain, point bar, channel, and boundary. We use forty vertical layers of the three-dimensional channel deposition as the TIs.

Fig. 5 shows five random selection realizations, and five TIs with a size of 150×200, accompanied by the probability maps of green channel of facies 2. For the high-curve channel of a meandering river, we also showed that our realization is highly consistent with the training images. We can perfectly reproduce different combinations of channel and point bars. Similarly, for sinuous channels, we can observe that there is a reasonable agreement between the realizations and TIs in the probability map in Fig. 6, a high probability in the middle of the channel, low probability at the edge of the channel. The red and black lines in the corresponding variogram and connectivity functions of channel facies 2 demonstrate that the realizations achieve a good consistency with the TIs with a maximum deviation of not more than 0.2 in Fig. 6. The slight fluctuation also demonstrates the deviation and variety of the realizations. The variograms of facies 0, 1, and 2 are supplemented in the appendix.

3.2. Delta facies (non-stationary facies)

The delta facies test case considers the 150×200 deltaic TIs (layer 3) depicted in Fig. 2(d), representing non-stationary sedimentary facies with obvious trends and directions. The TIs are deltaic deposits of two facies: floodplains with shale deposits, and channels with sand deposits. Delta sedimentary architecture is relatively complex, with high reservoir heterogeneity of obvious direction and trend (Feng et al., 2017b; Gao et al., 2020). Building an accurate delta reservoir model is a recognized problem and is very important (De Vries et al., 2009; Gengxin et al., 2015; Wang et al., 2022).

Fig. 7 displays five random selection realizations and five TIs with a size of 150×200, accompanied by the probability maps of yellow channel of facies 2. Visually, the realizations appear in line with the TIs.

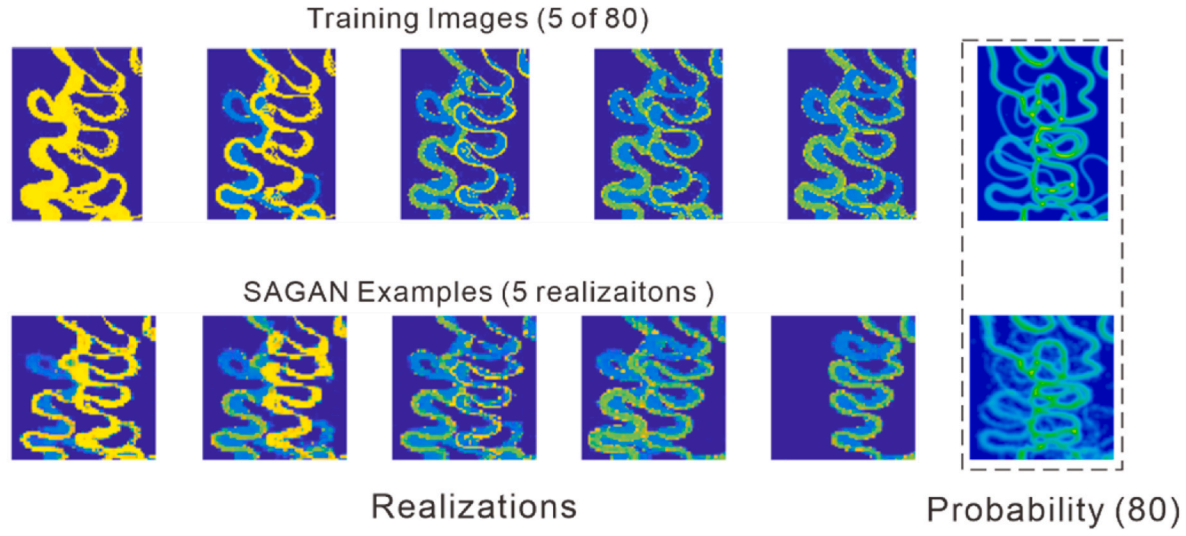

Fig. 5. Five randomly chosen TIs and realizations of meandering channels, along with corresponding probability maps of green channel facies.

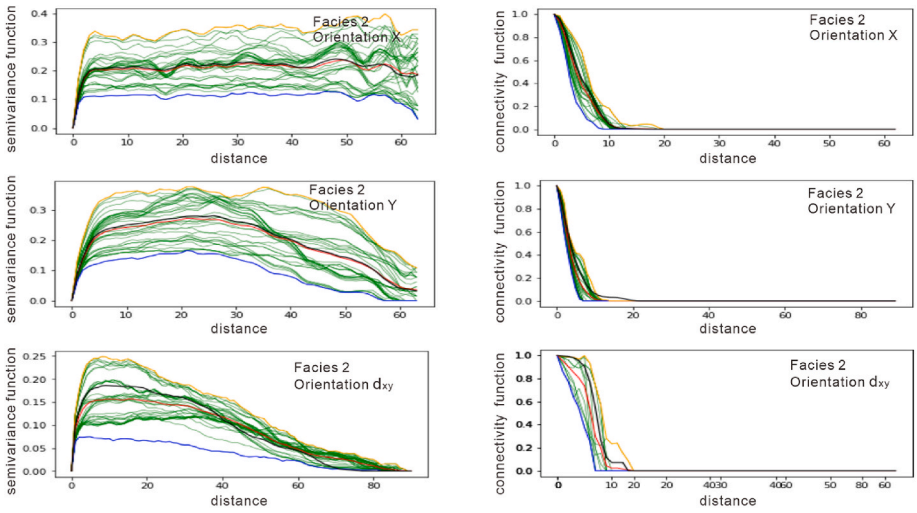

Fig. 6. Variograms and connectivity functions for the layer 2 meandering channels are depicted. The black line refers to the mean at each distance to 40 TIs of size 64 × 64 from the 200 × 150. The green lines are 40 realization of size 64 × 64, and the red lines are the mean of these green lines. The yellow and blue lines represent the maximum and minimum values of the function corresponding to the realizations. We calculate the functions for facies 2 along three main directions: x axis, y axis, and d_{XY} (45° direction). (For interpretation of the references to colour in this figure legend, the reader is referred to the Web version of this article.)

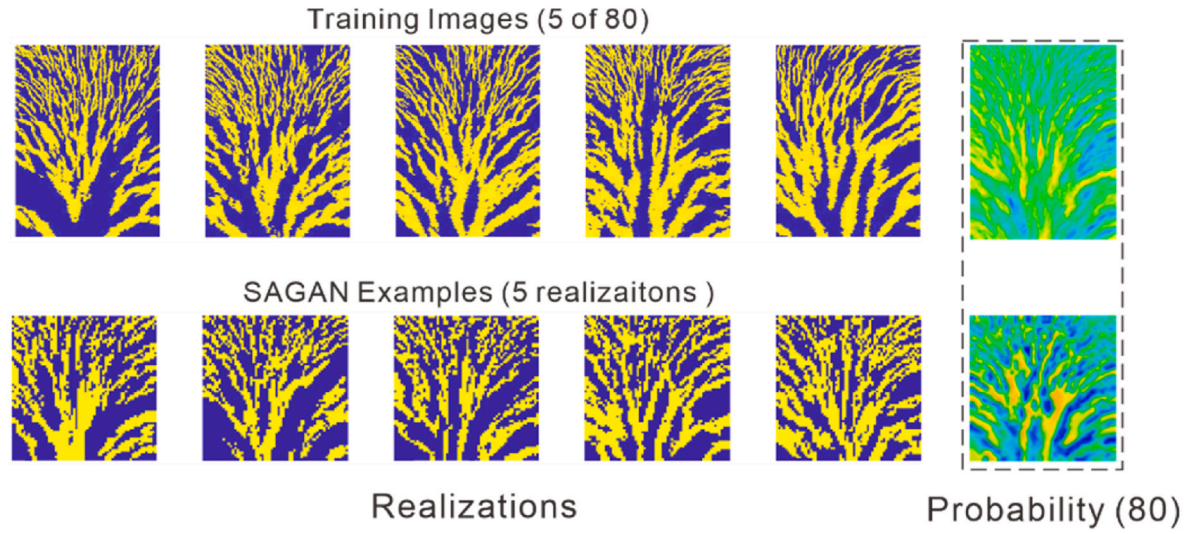

Fig. 7. Five randomly chosen TIs and realizations of delta, together with corresponding probability maps of yellow channel facies. (For interpretation of the references to colour in this figure legend, the reader is referred to the Web version of this article.)

The simulation realization realistically represents the characteristics of the outward divergence of the delta channel. The channel is wider and less branched at the root of the delta and gradually develops into multiple, smaller branches as the delta expands into the basin. The probability distribution also perfectly reproduces the extended trend of the delta. Fig. 8 shows the corresponding variogram and connectivity function metrics. The realizations match well with the statistics, and maximum absolute deviation is 0.2. This deviation shows wide diversity of simulation realizations.

To compare the geostatistics method and SAGAN method for non-stationary facies modeling, we simulate deltas with the SNESM method of MPS and SAGANs with the same TIs. Fig. 9 shows realizations of deltas simulated by basic MPS and SAGANs. SAGANs realizations reveal more realistic geometric features and depositional patterns of the channels in the delta. The MPS method has difficulty reproducing the divergent characteristics of the delta, with relative homogeneity.

To compare the differences between the GANs and SAGANs methods, we simulate deltas of different sizes with the basic GANs and SAGANs with the same TIs. Here, the basic GAN represents the most basic loss function and a simple generator and discriminator, without adding a self-attention mechanism, we used Laloy et al. (Laloy et al., 2017) GANs in our research. Fig. 10 shows realizations of different sizes of deltas simulated by the basic GANs(a) and SAGANs (b). SAGAN realizations reveal more realistic geometric features and depositional patterns of the channels in the delta, not limited to sizes as 32×32 or 128×128. In the realizations of the size of 128×128, we observe that the basic GANs only reproduce the non-stationary features of the delta locally (within the red frame), while the SAGANs can perfectly reproduce the global feature of the delta. As the realizations become more continuous and larger in size, the SAGAN method has improved results for large-scale modeling compared to the GAN method.

From the perspective of quantitative evaluation, the simulation realizations of the SAGAN method are closer to the training image than the basic GAN in variogram and connection functions. Regardless of the size of 32×32 (Fig. 11), 64×64 (Fig. 12) or 128×128 (Fig. 13), SAGAN's simulation results (green lines) float around the average value of the training images (red lines). Compared with SAGANs, the basic GANs simulation results are quite different from the training image average (red lines). All results show that SAGANs have more powerful modeling capabilities than basic GANs.

For the non-stationary delta case study, SAGAN method has obvious advantages over MPS and basic GAN in long-range dependency, and the realizations of this method can reproduce realistic TIs' features for non-stationary sedimentary facies with strong heterogeneity. For long-

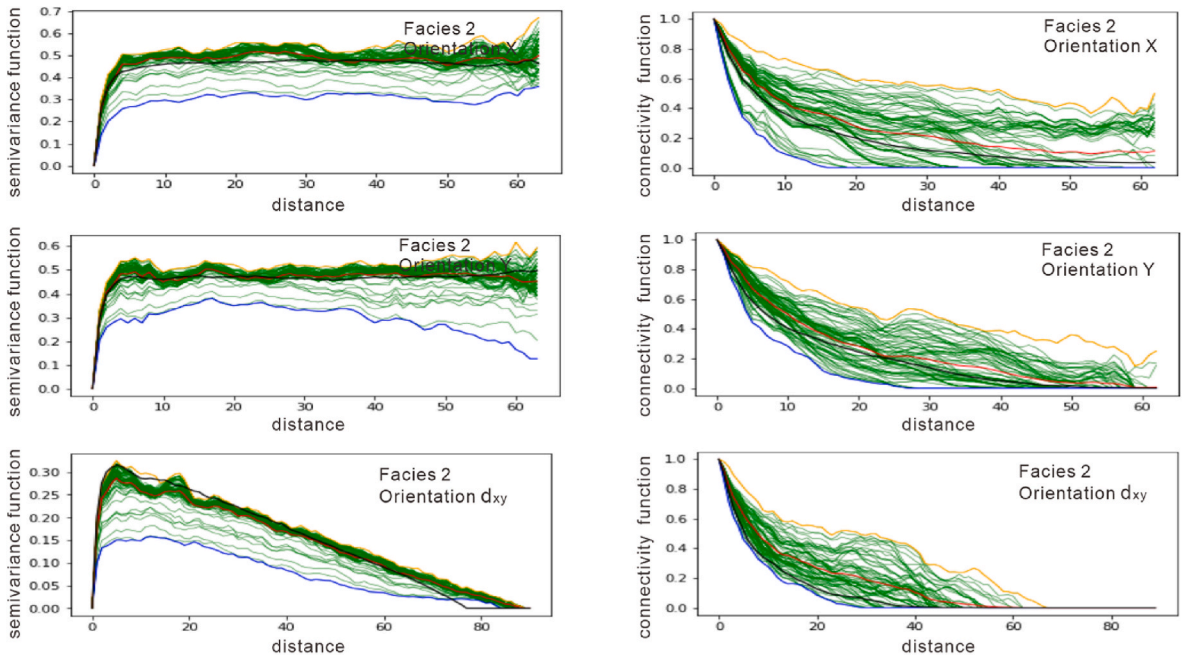

Fig. 8. Variograms and connectivity functions for the layer 3 delta depicted. The black line refers to the mean at each distance to 80 TIs of size 64× 64 from the 200 × 150. The green lines are 80 realizations of size 64 × 64, and the red lines are the mean of these green lines. The yellow and blue lines represent the maximum and minimum values of the function corresponding to the result. We calculate the variogram for facies 2 along three main directions: x axis, y axis, and d_{XY} (45° direction). (For interpretation of the references to colour in this figure legend, the reader is referred to the Web version of this article.)

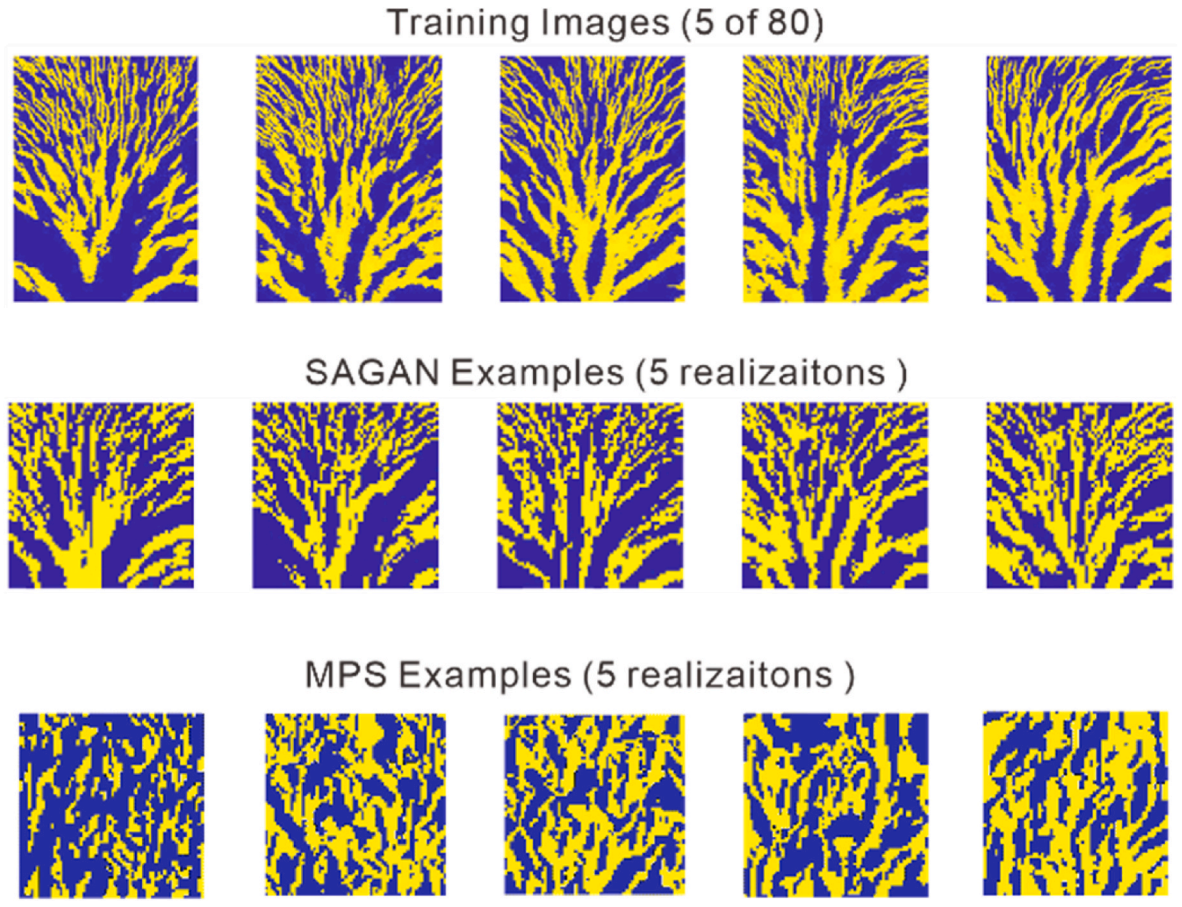

Fig. 9. Realizations of delta simulated by MPS and SAGANs.

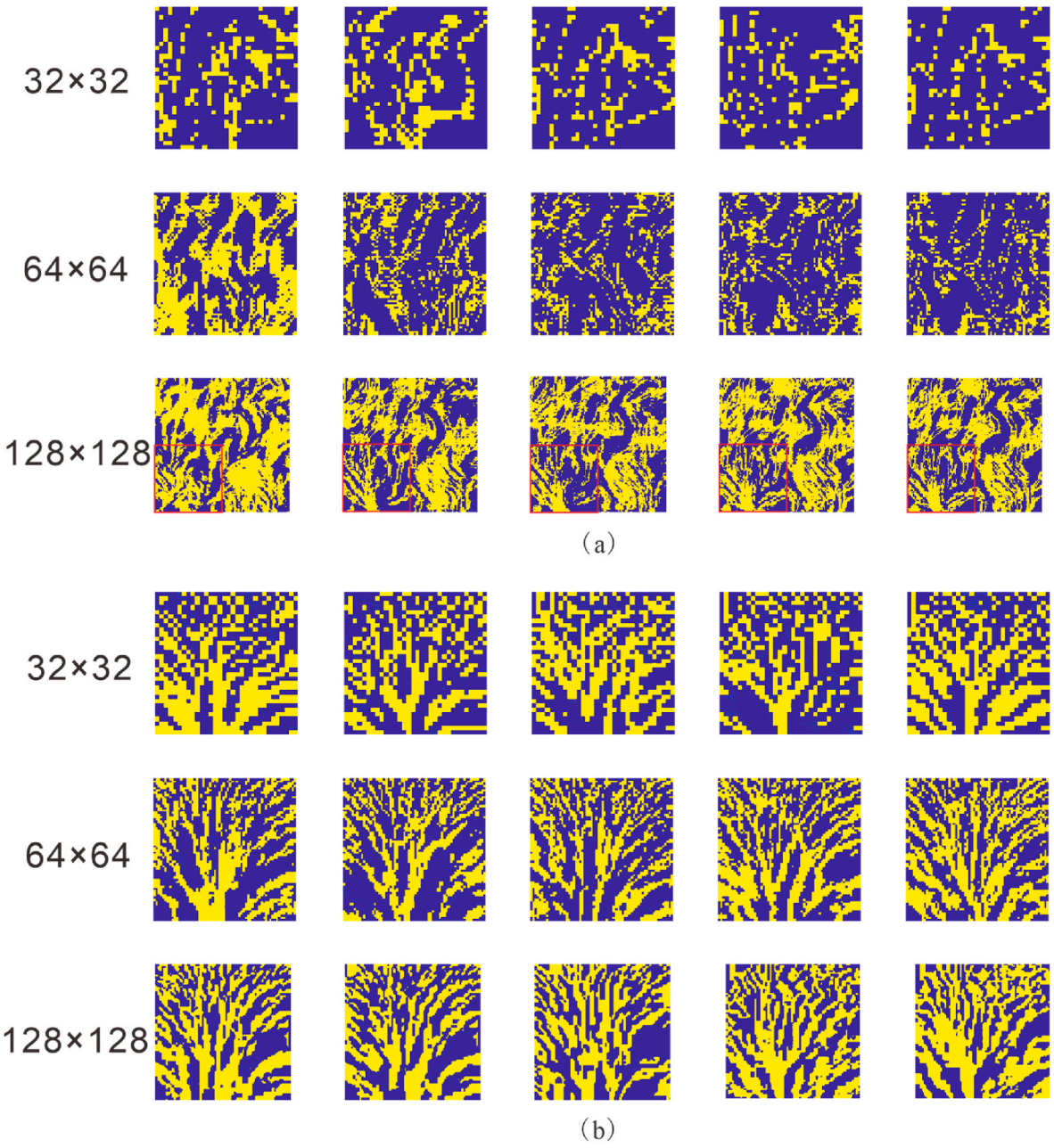

Fig. 10. Realizations of different sizes of deltas simulated by basic GANs (a) and realizations of different sizes of deltas simulated by SAGANs (b) of the same training images mentioned in Fig. 2.

distance and non-stationary features, we can reproduce the channels' expansion characteristics perfectly. We also achieve diversity, which contributes to the uncertainty evaluation of the reservoir.

4. Discussion

The applications above show that the SAGANs method is very effective for subsurface complex sedimentary facies modeling. Compared with existing GANs' sedimentary facies modeling study (Laloy et al., 2017; Zhang et al., 2019), the proposed SAGANs architecture solves an important issue: the self-attention module in the GANs framework is effective in modeling long-range dependencies and it can better reproduce the global spatial structure of sedimentary facies models, making up for the shortcomings of existing GAN modeling methods. (1) For the perspective of complex sedimentary facies modeling, especially delta facies modeling (Zhang, 2002; De Vries et al., 2009; Gengxin et al., 2015), we provide a new modeling method, which can solve the problem of distribution feature reproduction of non-stationary sedimentary facies. Our study confirms the effectiveness of SAGANs method in reproducing the spatial distribution features of the sedimentary facies than MPS (Fig. 9) and basic GANs (Laloy et al., 2017) (Figs. 10–13). This successful introduction of the SAGANs method to sedimentary facies modeling, demonstrates the potential of this machine learning method for sedimentary facies model characterization for complex sedimentary facies. (2) In the current research on the use of GAN for sedimentary facies modeling (Song et al., 2021a; Zhang et al., 2019), our research considers the modeling difficulties of complex sedimentary facies, and has made a successful attempt especially for non-stationary facies, which improves the application of GAN modeling methods and solve the problem of global feature reproduction of non-stationary sedimentary facies. Our study confirms the effectiveness of the self-attention mechanism in reproducing the global features of the

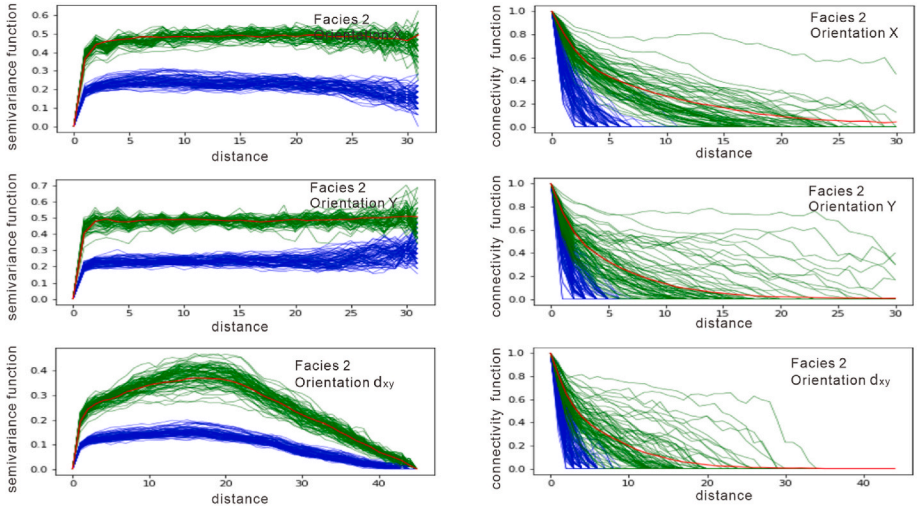

Fig. 11. Variograms and connectivity functions for the layer3 delta depicted. The black line refers the mean at each distance to 80 TIs of size 32×32 from the 200×150. The green lines are 40 realization of size 32×32. The yellow and blue lines represent the maximum and minimum values of the function corresponding to the result. We calculate the variogram for the facies 2 along three main directions: x axes, y axes, and d_{XY} (45° direction). (For interpretation of the references to colour in this figure legend, the reader is referred to the Web version of this article.)

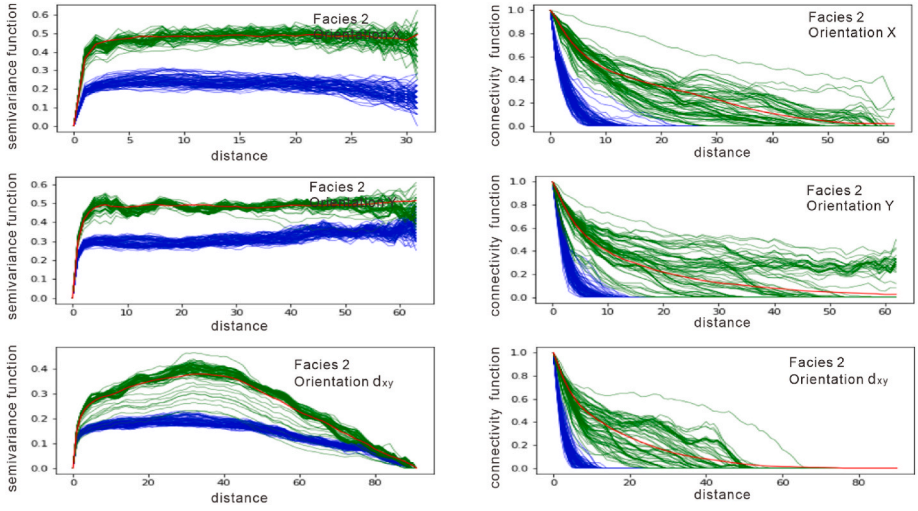

Fig. 12. Variograms and connectivity functions for the layer3 delta depicted. The black line refers the mean at each distance to 80 TIs of size 64×64 from the 200×150. The green lines are 40 realization of size 64×64. The yellow and blue lines represent the maximum and minimum values of the function corresponding to the result. We calculate the variogram for the facies 2 along three main directions: x axes, y axes, and d_{XY} (45° direction). (For interpretation of the references to colour in this figure legend, the reader is referred to the Web version of this article.)

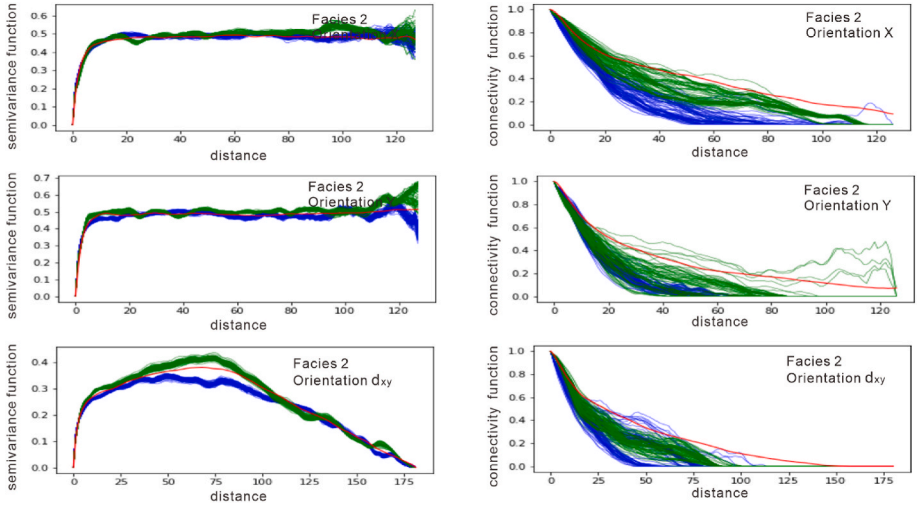

Fig. 13. Variograms and connectivity functions for the layer3 delta depicted. The black line refers the mean at each distance to 80 TIs of size 128×128 from the 200×150. The green lines are 40 realization of size 128×128. The yellow and blue lines represent the maximum and minimum values of the function corresponding to the result. We calculate the variogram for the facies 2 along three main directions: x axes, y axes, and d_{XY} (45° direction). (For interpretation of the references to colour in this figure legend, the reader is referred to the Web version of this article.)

training images, which can provide a new idea and method for the modeling of complex sedimentary facies. In addition, once the training is completed, the simulated SAGANs improve the speed for complex sedimentary facies (Laloy et al., 2017), even though the training aspect of the workflow takes several hours whereas producing a single realization only takes 0.04 s.

Current limitations of SAGANs are better understanding the conditionalization of the modeling (to match prior information, such as well data, seismic data, etc.) and three-dimensional modeling (Song et al., 2021b, 2021c), which are our future research directions. For conditional model, it can be achieved by modifying the loss function of SAGAN. For three-dimensional modeling of sedimentary facies, one can consider reconstructing three-dimensional space from two-dimensional planes (Coiffier et al., 2020; Wang et al., 2022; Song et al., 2021c). About simulation time, hardware improvement (GPU) can considerably speed up the training and further optimization of the network structure can enhance the SAGANs' simulation capability.

5. Conclusions

We present a new GAN-based modeling method for subsurface sedimentary facies: Self-Attention Generative Adversarial Networks (SAGANs). Compared with existing geostatistical and basic GAN methodologies, SAGAN's advantage is that the model realizations can capture TI statistics and enable long-range dependencies. This allows for efficiently modeling complex non-stationary TIs with strong heterogeneity. Several sedimentary facies cases have successfully examined the simulation quality of SAGAN-based approach, including stationary channels and non-stationary delta facies. For channel cases, realizations can reproduce the different distributions of channels and point bars in different river systems. For the delta case, the SAGAN method shows a better ability to reproduce delta divergence characteristics than the MPS and basic GANs. The generations are completely consistent with prior sedimentary facies depositional patterns, indicating that SAGANs represent a powerful method for reproducing prior sedimentary facies depositional patterns. Future research mainly includes realizing a direct adjustment of SAGANs simulations for conditioning data (well data, seismic data, etc.), improve simulation quality, adapt to 3-D simulation and speed up training time.

Credit author statement

Shenghe Wu and JiaJia Zhang provided funding for the project, and suggested to the manuscript. Heather Bedle helped modify and improve the manuscript. Pengfei Xie and Yunlong Wang assisted in generation quality assessment.

Declaration of competing interest

The authors declare that they have no known competing financial interests or personal relationships that could have appeared to influence the work reported in this paper.

Acknowledgments

Our research was funded by the National Natural Science Foundation of China (CN) (Nos. 41772101, 420021112), the Strategic Cooperation Technology Projects of CNPC and CUPB (No. ZLZX 2020-02) and China Postdoctoral Science Foundation (No. 2020M670580).

Appendix A. Supplementary data

Supplementary data to this article can be found online at https://doi.org/10.1016/j.petrol.2022.110470.

References

Bergen, K.J., Johnson, P.A., de Hoop, M.V., Beroza, G.C., 2019. Machine learning for data-driven discovery in solid Earth geoscience. Science 363 (6433) eaau0323. DOI: 10.1126/science.aau0323.

Caers, Zhang, T., 2002. Multiple-point geostatistics: a quantitative vehicle for integrating geologic analogs into multiple reservoir models. Aapg Memoir 80 (80), 383–394.

Canchumuni, S.W., Emerick, A.A., Pacheco, M.A.C., 2019. Towards a robust parameterization for conditioning facies models using deep variational autoencoders and ensemble smoother. Comput. Geosci. 128, 87–102. https://doi.org/10.1016/j.cageo.2019.04.006.

Castro, S., Caers, J., Mukerji, T., 2005. The Stanford VI Reservoir: 18th Annual Report. Stanford Center for Reservoir Forecasting, Stanford University.

Chan, S., Elsheikh, A.H., 2017. Parametrization and Generation of Geological Models with Generative Adversarial Networks arXiv arXiv:1708.01810.

Coiffier, G., Renard, P., Lefebvre, S., 2020. 3D geological image synthesis from 2D examples using generative adversarial networks. Frontiers in Water 2, 30. https://doi.org/10.3389/frwa.2020.560598.

De Vries, L., Carrera, J., Falivene, O., Gratacos, O., Slooten, L.J., 2009. Application of Multiple Point Geostatistics to Non-stationary Images. Math. https://doi.org/10.1007/s11004-008-9188-y.

Dupont, E., Zhang, T., Tilke, P., Liang, L., Bailey, W., 2018. Generating Realistic Geology Conditioned on Physical Measurements with Generative Adversarial Networks arXiv preprint arXiv:1802.03065.

Feng, W., Wu, S., Yin, Y., Zhang, J., Zhang, K., 2017a. A training image evaluation and selection method based on minimum data event distance for multiple-point geostatistics. Comput. Geosci. 104, 35–53. https://doi.org/10.1016/j.cageo.2017.04.004.

Feng, W.J., Wu, S.H., Zhang, K., Zhao, W., Jia, F., 2017b. Depositional process and sedimentary model of meandering-river shallow delta: insights from numerical simulation and modern deposition. Acta Geol. Sin. 91 (9), 2047–2064.

Gao, X., He, W., Hu, Y., 2020. Modeling of meandering river deltas based on the conditional generative adversarial network. J. Petrol. Sci. Eng. 193, 107352. https://doi.org/10.1016/j.petrol.2020.107352.

Gengxin, C.H.E.N., Fan, Z.H.A.O., Jiangong, W.A.N.G., Zheng, H., Yaozu, Y.A.N., Aiping, W.A.N.G., et al., 2015. Regionalized multiple-point stochastic geological modeling: a case from braided delta sedimentary reservoirs in Qaidam Basin, NW China. Petrol. Explor. Dev. 42 (5), 697–704. https://doi.org/10.1016/S1876-3804(15)30065-3.

Goodfellow, I., Pouget-Abadie, J., Mirza, M., Xu, B., Warde-Farley, D., Ozair, S., et al., 2014. Generative adversarial nets. Adv. Neural Inf. Process. Syst. 27.

Karras, T., Aila, T., Laine, S., Lehtinen, J., 2017. Progressive Growing of Gans for Improved Quality, Stability, and Variation arXiv preprint arXiv:1710.10196.

Kingma, D.P., Ba, J., 2014. Adam: A Method for Stochastic Optimization. arXiv preprint arXiv:1412.6980.

Kingma, D.P., Welling, M., 2013. Auto-encoding Variational Bayes arXiv preprint arXiv:1312.6114.

Laloy, E.N., Linde, D., Jacques, G., Mariethoz, G., 2016. Merging parallel tempering with sequential geostatistical resampling for improved posterior exploration of high-dimensional subsurface categorical fields. Adv. Water Resour. 90, 57–69. https://doi.org/10.1016/j.advwatres.2016.02.008.

Laloy, E., Hérault, R., Lee, J., Jacques, D., Linde, N., 2017. Inversion using a new low-dimensional representation of complex binary geological media based on a deep neural network. Adv. Water Resour. 110, 387–405. https://doi.org/10.1016/j.advwatres.2017.09.029.

Lee, J., Mukerji, T., 2012. The Stanford VI-E reservoir: a synthetic data set for joint seismic-EM time-lapse monitoring algorithms. In: 25th Annual Report, Stanford Center for Reservoir Forecasting. Stanford University.

Li, X., Mariethoz, G., Lu, D.T., Linde, N., 2016. Patch-based iterative conditional geostatistical simulation using graph cuts. Water Resour. Res. 52, 6297–6320. https://doi.org/10.1002/2015WR018378.

Liu, Y., Guo, C., Cao, J., Cheng, Z., Ding, X., Lv, L., et al., 2020. A new resolution enhancement method for sandstone thin-section images using perceptual GAN. J. Petrol. Sci. Eng. 195, 107921. https://doi.org/10.1016/j.petrol.2020.107921.

Mariethoz, G., Renard, P., Straubhaar, J., 2010. The direct sampling method to perform multiple-point geostatistical simulations. Water Resour. Res. 46 (11) https://doi.org/10.1029/2008WR007621.

Mosser, L., Dubrule, O., Blunt, M.J., 2017. Reconstruction of three-dimensional porous media using generative adversarial neural networks. Phys. Rev. 96 (4), 043309 https://doi.org/10.1103/PhysRevE.96.043309.

Mosser, L., Dubrule, O., Blunt, M.J., 2018. Stochastic reconstruction of an oolitic limestone by generative adversarial networks. Transport Porous Media 125 (1), 81–103. https://doi.org/10.1007/s11242-018-1039-9.

Radford, A., Metz, L., Chintala, S., 2015. Unsupervised Representation Learning with Deep Convolutional Generative Adversarial Networks arXiv preprint arXiv:1511.06434.

Song, S., Mukerji, T., Hou, J., 2021a. GANSim: conditional facies simulation using an improved progressive growing of generative adversarial networks (GANs). Math. Geosci. 53 (7), 1413–1444. https://doi.org/10.1007/s11004-021-09934-0.

Song, S., Mukerji, T., Hou, J., 2021b. Bridging the gap between geophysics and geology with generative adversarial networks. IEEE Trans. Geosci. Rem. Sens. 60, 1–11. https://doi.org/10.1109/TGRS.2021.3066975.

Song, S., Mukerji, T., Hou, J., 2021c. Geological facies modeling based on progressive growing of generative adversarial networks (GANs). Comput. Geosci. 25 (3), 1251–1273. https://doi.org/10.1007/s10596-021-10059-w.

Song, S., Mukerji, T., Hou, J., Zhang, D., Lyu, X., 2021d. GANSim-3D for Conditional Geomodelling: Theory and Field Application. https://doi.org/10.31223/X5FK8B.

Strebelle, S., 2002. Conditional simulation of complex geological structures using multiple-point statistics. Math. Geol. 34 (1), 1–21. https://doi.org/10.1023/A:1014009426274.

Tian, M., Xu, H., Cai, J., Wang, J., Wang, Z., 2019. Artificial neural network assisted prediction of dissolution spatial distribution in the volcanic weathered crust: a case

study from Chepaizi bulge of Junggar basin, northwestern China. Mar. Petrol. Geol. 110, 928–940. https://doi.org/10.1016/j.marpetgeo.2019.08.045.

Veillard, A., Morère, O., Grout, M., Gruffeille, J., 2018. Fast 3D seismic interpretation with unsupervised deep learning: application to a potash network in the north sea. In: 80th EAGE Conference and Exhibition 2018. https://doi.org/10.3997/2214-4609.201800738.

Wang, X., Girshick, R., Gupta, A., He, K., 2018. Non-local neural networks. In: Proceedings of the IEEE Conference on Computer Vision and Pattern Recognition, pp. 7794–7803.

Wang, L., Yin, Y., Zhang, C., Feng, W., Li, G., Chen, Q., Chen, M., 2022. A MPS-based novel method of reconstructing 3D reservoir models from 2D images using seismic constraints. J. Petrol. Sci. Eng. 209, 109974. https://doi.org/10.1016/j.petrol.2021.109974.

Wu, J., Zhang, T., Boucher, A., 2007. Non-stationary Multiple-point Geostatistical Simulations with Region Concept.

Zhang, T., 2002. Rotation and affinity invariance in multiple-point geostatistics, 94305-2220. In: SCRF Annual Meeting Report, vol. 15.

Zhang, H., Goodfellow, I., Metaxas, D., Odena, A., 2019. May. Self-attention generative adversarial networks. In: International Conference on Machine Learning. PMLR, pp. 7354–7363.

Zhang, T., Tilke, P., Dupont, E., Zhu, L., Liang, L., Bailey, W., 2019. March. Generating geologically realistic 3D reservoir facies models using deep learning of sedimentary architecture with generative adversarial networks. In: International Petroleum Technology Conference. OnePetro. https://doi.org/10.2523/IPTC-19454-MS.

Zhang, C., Song, X., Azevedo, L., 2021. U-net generative adversarial network for subsurface facies modeling. Comput. Geosci. 25 (1), 553–573.

Zhu, L., Zhang, T., 2019. Generating Geological Facies Models with Fidelity to Diversity and Statistics of Training Images Using Improved Generative Adversarial Networks arXiv preprint arXiv:1909.10652.